Magnetic ordering in $ErFe_6Sn_6$

2003 J. Phys.: Condens. Matter 15 1757

(http://iopscience.iop.org/0953-8984/15/10/322)

INSTITUTE OF PHYSICS PUBLISHING JOURNAL OF PHYSICS: CONDENSED MATTER

J. Phys.: Condens. Matter **15** (2003) 1757–1771 PII: S0953-8984(03)57075-8

Magnetic ordering in $ErFe_6Sn_6$

J M Cadogan[1,5], D H Ryan[2], O Moze[3], Suharyana[1] and M Hofmann[4,6]

[1] School of Physics, The University of New South Wales, Sydney NSW 2052, Australia
[2] Department of Physics and Centre for the Physics of Materials, McGill University, Montreal, H3A 2T8, Canada
[3] Istituto Nazionale per la Fisica della Materia, Dipartimento di Fisica, Università di Modena e Reggio Emilia, Via G Campi 213/a, I-41100, Modena, Italy
[4] Hahn-Meitner Institute, BENSC, Glienickerstraße 100, 14109 Berlin, Germany

E-mail: j.cadogan@unsw.edu.au

Received 3 December 2002
Published 3 March 2003
Online at stacks.iop.org/JPhysCM/15/1757

Abstract

We have determined the magnetic structures of the Er and Fe sublattices in $ErFe_6Sn_6$ by high-resolution neutron powder diffraction and Mössbauer spectroscopy on the ^{166}Er, ^{57}Fe and ^{119}Sn isotopes. The crystal space group is orthorhombic $Cmcm$. The Fe sublattice is antiferromagnetic with a Néel temperature of 560(5) K and it orders along the [100] direction with a magnetic space group $C_Pm'c'm'$ and a propagation vector [010]. The Fe magnetic moment at 1.5 K is $2.4 \pm 0.6\ \mu_B$. The Er sublattice orders independently of the Fe sublattice at 4.8 ± 0.4 K and comprises a ferromagnetic mode along [100] and an antiferromagnetic mode along [010], with a propagation vector $[0\frac{1}{2}0]$ i.e. cell-doubling along [010]. The magnetic space group of the Er sublattice within the magnetic unit cell is $Pbc'm'$, a subgroup of $Cmcm$. At 1.5 K the ferromagnetic and antiferromagnetic components of the Er^{3+} magnetic moment (determined by a combination of neutron diffraction and magnetization measurements) are 5.9 ± 0.1 and $4.9 \pm 1.5\ \mu_B$, respectively, yielding a net Er moment of $7.7 \pm 1.5\ \mu_B$. The Er^{3+} magnetic moment derived from ^{166}Er Mössbauer spectroscopy is $8.5(1)\ \mu_B$.

1. Introduction

The magnetic moments on the rare-earth (R) and Fe sublattices in the RFe_6Ge_6 and RFe_6Sn_6 intermetallic compounds order independently of one another in those compounds where the R^{3+} ion has a magnetic moment [1–4]. The Fe sublattice orders antiferromagnetically with a Néel temperature (T_N) which remains essentially constant across a series with $T_N \sim 485$ K in

[5] Author to whom any correspondence should be addressed.
[6] Present address: FRM-II, Technische Universität München, D-85747 Garching, Germany.

RFe_6Ge_6 and ∼555 K in RFe_6Sn_6. Neutron powder diffraction shows that the easy direction of magnetic order of the Fe sublattice is [100] in the orthorhombic setting [5–8].

For R = Gd–Er, the rare-earth sublattice orders at much lower temperatures, ranging from 45 K for $GdFe_6Sn_6$ to 3 K for $ErFe_6Ge_6$, without affecting the Fe order. The magnetic independence of the R and Fe sublattices is related to the layered structure of these compounds which are formed by placing rare-earth atoms between the hexagonal Fe planes of the parent FeGe or FeSn (B35) structure. Binary FeGe/FeSn consists of ferromagnetic Fe planes coupled antiferromagnetically to each other [9, 10] and there is a net cancellation of the Fe–R magnetic exchange at the interplanar R sites in RFe_6Ge_6 and RFe_6Sn_6, effectively isolating the rare-earth from the ordering of the iron moments. The magnetic ordering of the R sublattice in RFe_6Ge_6 and RFe_6Sn_6, two orders of magnitude lower in temperature than the Fe ordering, is most likely the result of an RKKY-type coupling between R moments. The magnetic behaviour of these series of compounds has recently been reviewed by Cadogan and Ryan [11].

In this paper we determine the magnetic structures of the Er and Fe sublattices in $ErFe_6Sn_6$ using high-resolution neutron powder diffraction, complemented by ^{166}Er, ^{57}Fe and ^{119}Sn Mössbauer spectroscopy.

2. Experimental methods

The $ErFe_6Sn_6$ sample was prepared by arc-melting stoichiometric amounts of the pure elements under Ti-gettered argon. The sample was subsequently annealed at 850 °C for two weeks, sealed under vacuum in a quartz tube. Powder x-ray diffraction was carried out using Cu Kα radiation on an automated Nicolet-Stoe diffractometer. The Néel temperature of the Fe sublattice in $ErFe_6Sn_6$ was measured by differential scanning calorimetry (DSC), at a heating rate of 40 K min^{-1}, on a Perkin-Elmer DSC-7, using the heat capacity peak at T_N to signal magnetic ordering. Magnetization and ac susceptibility were measured on a Quantum Design PPMS.

^{57}Fe and ^{119}Sn Mössbauer spectroscopy was carried out in conventional, constant-acceleration, transmission mode with standard ^{57}CoRh and ^{119m}Sn:$BaSnO_3$ sources, respectively. In both cases, the spectrometer was calibrated against a 99.99% α-Fe foil and the ^{57}CoRh source.

The source for the ^{166}Er Mössbauer spectroscopy was made by neutron irradiation of $Ho_{0.4}Y_{0.6}H_2$ at the SLOWPOKE Reactor Laboratory, Ecole Polytechnique Montréal, to produce ∼1 GBq initial activity of the 27 h ^{166}Ho parent isotope. The ^{166}Er spectrum was obtained at 2 K in a helium-flow cryostat and the source was heated to ∼5 K to avoid line broadening. The 80.6 keV ^{166}Er gamma rays were detected using a high-purity germanium detector. The spectrometer was operated in sine mode and calibrated using the 819.4 T magnetic splitting in $ErFe_2$ at 1.4 K. This calibration field is the average of the ^{166}Er Mössbauer measurement of 820.5(8) T by Hodges *et al* [12] and the ^{167}Er NMR measurement of 818.4 ± 10 T by Berthier and Devine [13]. (It is implicit here that the so-called *hyperfine anomaly*, which can give rise to very small differences in the hyperfine fields experienced by different isotopes, is negligible. In any event, such a difference is probably within the experimental error of these field determinations.) The source linewidth on the $ErFe_2$ calibration was 2.49(4) mm s^{-1} and the spectrum was fitted using a non-linear least squares routine to the full nuclear hyperfine Hamiltonian. To facilitate comparison with other techniques we note that a Mössbauer *splitting* of 1 mm s^{-1} in ^{166}Er corresponds to 64.973 MHz, 43.052×10^{-27} J or 3.1182 mK.

Neutron powder diffraction experiments were carried out on ∼6 g samples on the E9 fine resolution powder diffractometer (FIREPOD) at the BENSC reactor, Hahn–Meitner

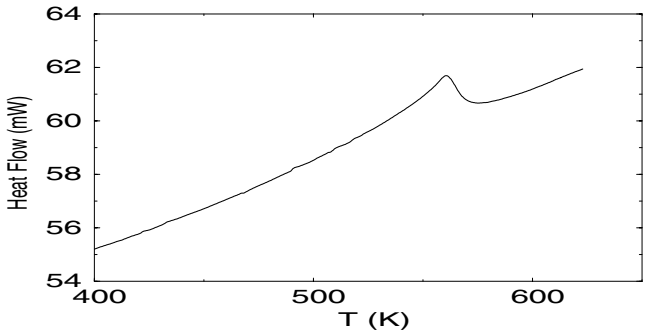

Figure 1. DSC trace of $ErFe_6Sn_6$ obtained at a heating rate of 40 K min^{-1}.

Institute, Berlin, Germany. The neutron wavelength was 1.5831(1) Å. A detailed description of FIREPOD has been published by Többens and Stüßer [14]. An additional pattern at a longer wavelength of 2.447(1) Å was obtained on the E6 focusing diffractometer at BENSC. All diffraction patterns were analysed using the Rietveld method and the GSAS program [15]. The symmetry-related restrictions placed on the allowed magnetic structures of the Er sublattice in $ErFe_6Sn_6$ were checked using the SARA*h* representational analysis program of Wills [16].

3. Results and discussion

3.1. Crystal structure

The annealed sample of $ErFe_6Sn_6$ was virtually single phase with a trace of $ErSn_3$ present in an amount <2 wt%, as determined from the fits to the neutron diffraction patterns. The crystal structure of $ErFe_6Sn_6$ is orthorhombic with the space group *Cmcm* (no 63), in agreement with the work of Chafik El Idrissi *et al* [17]. There are two Er sites, five Fe sites and ten Sn sites. The lattice parameters and atomic positions of $ErFe_6Sn_6$ were determined by high-resolution neutron powder diffraction at 5.3 K. The lattice parameters are $a = 8.8737(4)$ Å, $b = 37.1808(29)$ Å and $c = 5.3780(4)$ Å. The conventional refinement R-factors (%) are $R(\text{Bragg}) = 8.6$, $R(\text{F-struct.}) = 7.7$, $R(\text{wp}) = 6.9$, $R(\text{exp}) = 2.1$ and $R(\text{mag}) = 11.9$. The refined atomic position parameters are given in table 1. During the neutron diffraction fitting procedure we employed three refinable isotropic thermal parameters (U_{iso}), one for each element, rather than trying to refine individual U_{iso} values for each of the 17 atomic sites in the $ErFe_6Sn_6$ structure. The refined values of U_{iso} at 5.3 K are 0.0173(22), 0.0064(7) and 0.0011(8) $Å^2$ for Er, Fe and Sn, respectively.

3.2. Magnetic ordering

In figure 1 we show the DSC trace of $ErFe_6Sn_6$. The Néel temperature of the Fe sublattice is 560(5) K, which compares well with the value of 553 K determined by Rao [18]. Our previously determined Néel temperature of the Fe sublattice in YFe_6Sn_6 is 558(5) K [8], consistent with the fact that the R^{3+} ion has effectively no influence on the ordering of the Fe sublattice.

In figure 2 we show the in-phase and out-of-phase components of the ac susceptibility of $ErFe_6Sn_6$ obtained at a frequency of 377 Hz and an ac magnetic field of 45 A m^{-1} (RMS). The magnetic ordering of the Er sublattice below 5 K is clear. The peak in $\chi_{ac}(T)$ occurs at 3.3 K and the deviation from linear Curie–Weiss behaviour commences at 4.6 K.

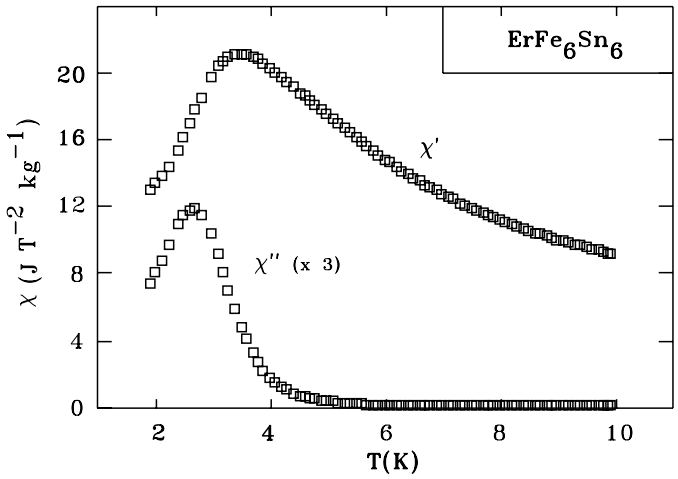

Figure 2. In-phase (χ') and out-of-phase (χ'') components of the ac susceptibility of $ErFe_6Sn_6$, measured at 377 Hz and 45 A m^{-1} (RMS).

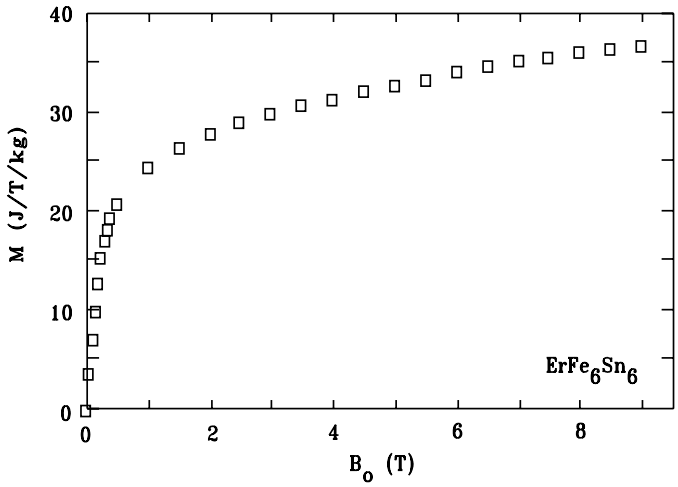

Figure 3. Magnetization of $ErFe_6Sn_6$ obtained at 2 K.

In figure 3 we show the magnetization of a powder sample of $ErFe_6Sn_6$ measured at 2 K in magnetic fields up to 9 T. The variation of the magnetization with applied field suggests that the Er sublattice order comprises both ferromagnetic and antiferromagnetic components. The spontaneous magnetization of $ErFe_6Sn_6$ at 2 K, derived by extrapolating the magnetization to zero applied field, is 27.2(5) J T kg^{-1}, which corresponds to an Er sublattice ferromagnetic component/formula unit (fu) of 5.9(1) μ_B/fu and hence an Er^{3+} ferromagnetic component of 5.9(1) μ_B at 2 K. Rao [18] determined a magnetization of 5.3(1) μ_B/fu from an extrapolation of magnetization data at 1.7 K, obtained in applied fields up to 5 T.

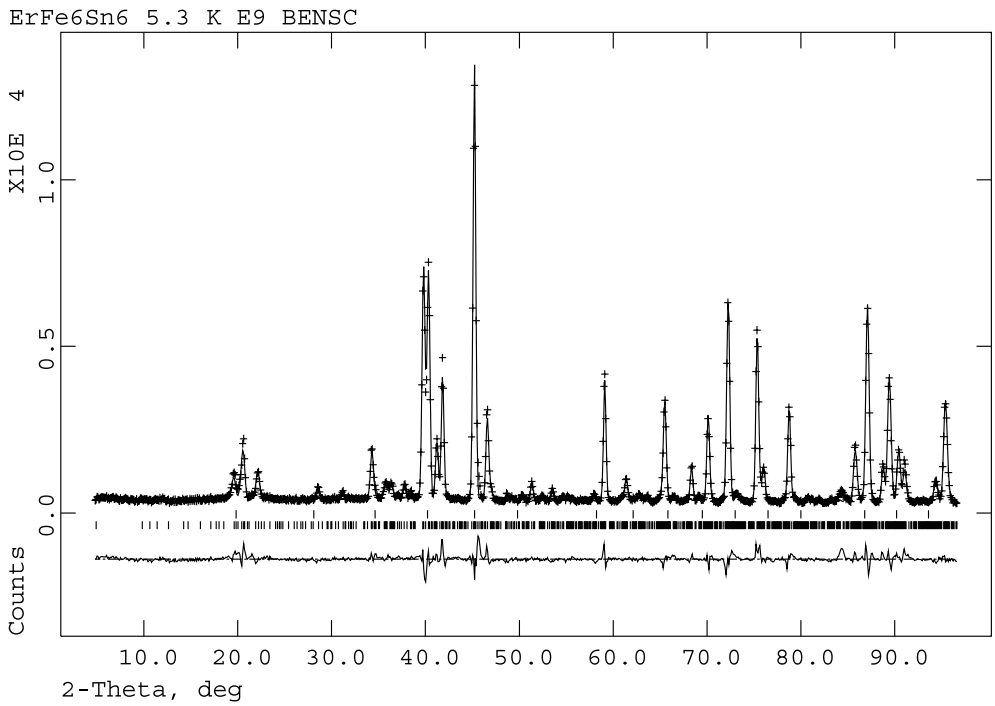

Figure 4. Neutron powder diffraction pattern of $ErFe_6Sn_6$ obtained at 5.3 K with $\lambda = 1.5831(1)$ Å. The Bragg position markers represent (top) the $ErSn_3$ impurity phase and (bottom) the $ErFe_6Sn_6$ nuclear and Fe magnetic scattering, respectively.

3.3. Neutron diffraction

3.3.1. Fe sublattice ordering. In figure 4 we show the neutron powder diffraction pattern of $ErFe_6Sn_6$ obtained at 5.3 K, at which temperature only the Fe sublattice is magnetically ordered.

As in the case of YFe_6Ge_6 [7], which has the same crystal space group ($Cmcm$) as $ErFe_6Sn_6$, the magnetic ordering of the Fe sublattice in $ErFe_6Sn_6$ results in the appearance of extra peaks with the condition $h + k = odd$ (nuclear scattering peaks obey $h + k = even$ for the $Cmcm$ space group). This is most clearly illustrated by the appearance of a strong, purely magnetic, (120) peak at $2\theta = 21°$. Thus, we describe the Fe order as *anti-C* i.e. Fe moments related by the C translation $+(\frac{1}{2}\frac{1}{2}0)$ are antiparallel.

We described the procedure for determining the magnetic ordering mode of the Fe sublattice in the $Cmcm$ space group in detail in our paper on YFe_6Ge_6 [7] and we refer the reader to our previous work. The reader is also referred to the comprehensive treatment of the $Cmcm$ space group by Prandl [19].

We obtained the best fit to the 5.3 K neutron diffraction pattern of $ErFe_6Sn_6$ with the Fe moments placed along the [100] direction with a propagation vector [010]. This ordering is a common feature of the RFe_6Ge_6 and RFe_6Sn_6 series [5–8]. The refined Fe magnetic moment in $ErFe_6Sn_6$ at 5.3 K is 2.4(6) μ_B. The magnetic space group of the Fe sublattice in $ErFe_6Sn_6$ is antiferromagnetic $C_Pm'c'm'$.

As in our previous studies of YFe_6Sn_6 [8] and $HoFe_6Sn_6$ [20], we have used ^{119}Sn Mössbauer spectroscopy to confirm the Fe sublattice magnetic ordering mode deduced from

Table 1. Atomic positions in $ErFe_6Sn_6$.

Atom	Site	x	y	z
Er	4c	0	0.8086(11)	1/4
Er	4c	0	0.0680(9)	1/4
Fe	8d	1/4	1/4	0
Fe	8e	0.2437(22)	0	0
Fe	8g	0.2473(25)	0.1899(6)	1/4
Fe	8g	0.2519(15)	0.4386(7)	1/4
Fe	16h	0.2497(16)	0.1254(5)	0.0129(30)
Sn	4c	0	0.2282(13)	1/4
Sn	4c	0	0.7246(11)	1/4
Sn	4c	0	0.1453(12)	1/4
Sn	4c	0	0.6456(12)	1/4
Sn	4c	0	0.8972(13)	1/4
Sn	4c	0	0.3983(13)	1/4
Sn	4c	0	0.4777(14)	1/4
Sn	4c	0	0.9770(12)	1/4
Sn	8g	0.3414(23)	0.8124(8)	1/4
Sn	8g	0.3279(23)	0.0578(6)	1/4

our neutron scattering experiments and we will present this argument in section 3.4.2 during our discussion of our Mössbauer work on $ErFe_6Sn_6$.

3.3.2. Er sublattice ordering. In figure 5 we show the neutron powder diffraction pattern of $ErFe_6Sn_6$ obtained at 1.5 K. The degree of magnetic scattering is very weak and the appearance of extra peaks associated with the magnetic ordering of the Er sublattice is only clear at $2\theta = 11.95°$.

In figure 6 we show a section of our set of neutron diffraction patterns obtained in the temperature range 1.8–5.3 K. The development of the purely magnetic $(1\frac{5}{2}0)$ peak at $2\theta \sim 12°$, arising from the antiferromagnetic order of the Er sublattice, is clear, albeit weak. The peak at $2\theta \sim 21°$ is the purely magnetic (120) peak, arising from the antiferromagnetic order of the Fe sublattice (which occurs at 560(5) K). The purely magnetic $(1\frac{5}{2}0)$ peak at $2\theta = 11.95°$ indicates a doubling of the magnetic cell along the crystal *b*-axis, associated with the antiferromagnetic component of the Er order. There are also magnetic contributions to nuclear peaks and the combination of our neutron scattering and magnetization data shows that the Er magnetic order comprises both ferromagnetic and antiferromagnetic components, a situation similar to that recently found in $HoFe_6Sn_6$ [20]. In figure 7 we show the integrated intensity of the $(1\frac{5}{2}0)$ peak as a function of temperature. These data show that the Er sublattice magnetic ordering occurs between 4.3 and 5.3 K and we therefore take the ordering temperature of the Er sublattice in $ErFe_6Sn_6$ to be 4.8(4) K.

As shown by Prandl [19], all of the magnetic space groups directly derived from the crystal space group *Cmcm* yield purely uniaxial magnetic modes, either ferromagnetic or antiferromagnetic, at the Er 4c site. Thus, one possible approach to the treatment of the Er magnetic order would involve the Er order belonging to two different representations of the *Cmcm* family, one ferromagnetic and one antiferromagnetic. The assignment of the Er order to two different *Cmcm*-type representations is not without precedent and the reader is referred to the classic paper on $ErCrO_3$ by Bertaut and Mareschal [21] and the review by Bertaut [22] for a discussion of this phenomenon. Furthermore, García-Matres *et al* [23] recently observed such mixing of irreducible representations in Tm_2BaNiO_5 and they pointed out that about 10%

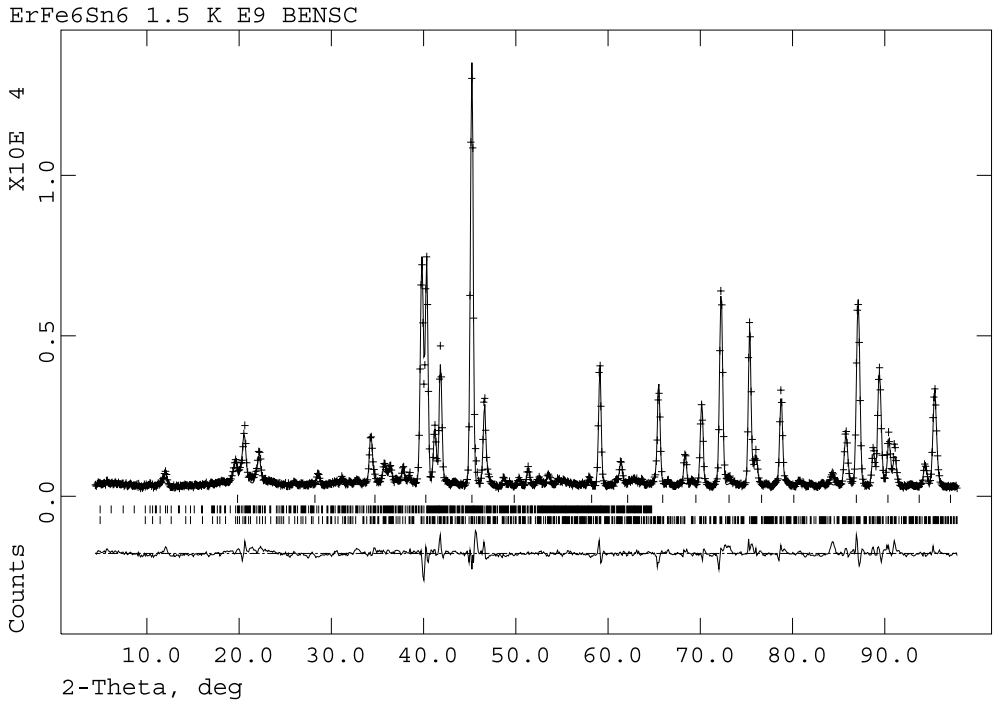

Figure 5. Neutron powder diffraction pattern of $ErFe_6Sn_6$ obtained at 1.5 K with $\lambda = 1.5831(1)$ Å. The Bragg position markers represent (top to bottom) the $ErSn_3$ impurity phase, the $ErFe_6Sn_6$ Er magnetic scattering and the $ErFe_6Sn_6$ nuclear and Fe magnetic scattering, respectively.

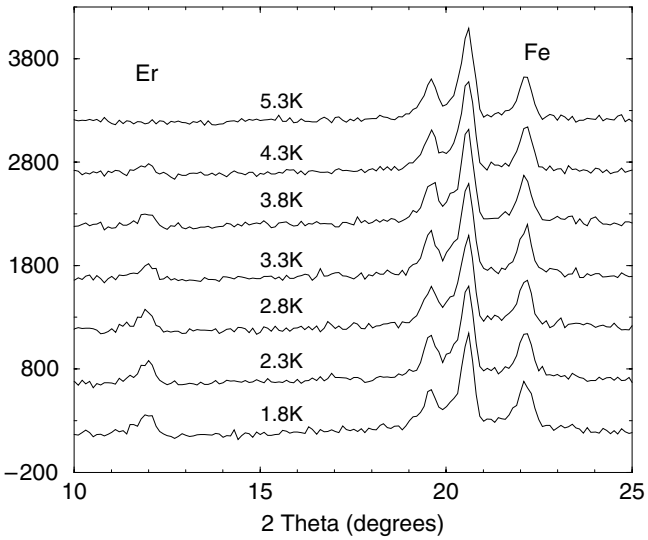

Figure 6. Sections of the neutron powder diffraction patterns of $ErFe_6Sn_6$ obtained in the temperature range 1.8–5.3 K with $\lambda = 1.5831(1)$ Å. The peak marked 'Er' is the purely antiferromagnetic $(1\frac{5}{2}0)$ peak from the Er sublattice and the peak marked 'Fe' is the purely antiferromagnetic $(12\bar{0})$ peak from the Fe sublattice.

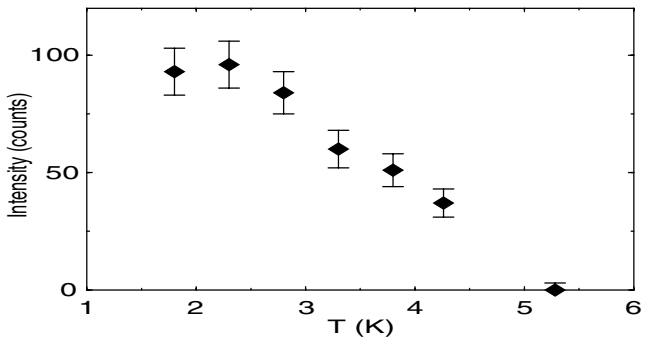

Figure 7. Temperature dependence of the integrated intensity of the antiferromagnetic $(1\frac{5}{2}0)$ Er peak in $ErFe_6Sn_6$.

of the magnetic structures listed in the 1976 compendium of magnetic structure by Olés *et al* [24] are mixed representations.

Alternatively, one may consider the Er sublattice order in a lower-symmetry space group than $Cmcm$. The cell doubling corresponds to a loss of the C translation of the underlying crystal space group and the magnetic space group must be of lower symmetry than the crystal group $Cmcm$. In an attempt to find a space group to *produce* the two groups of eight Er sites in the doubled magnetic cell we considered the orthorhombic space groups which are numbers 16–74 in the *International Tables for Crystallography* [25]. We can rule out those groups with fewer than eight general positions since each Er 4c site produces eight atoms in the doubled cell. Secondly, we may rule out all but 16 of the remaining groups due to the absence of C, I, A and F translations among these eight Er atomic positions. At this point we are left with groups 47–62 and the need for a $+(0\frac{1}{2}0)$ translation leaves only five groups, namely $Pnna$ (52), $Pccn$ (56), $Pbcm$ (57), $Pbca$ (61) and $Pnma$ (62). Unfortunately, none of these groups has a suitable site with the required multiplicity of eight.

However, if we subdivide the eight Er sites arising from the doubling of a crystal 4c site into two groups of four, one group in the $x = 0$ plane and the other in the $x = \frac{1}{2}$ plane, then each site is represented by the atomic positions (x, y, z), $(-x, \frac{1}{2}+y, z)$, $(x, \frac{1}{2}-y, \frac{1}{2}+z)$ and $(-x, -y, \frac{1}{2}+z)$ which is the 4d site in the $Pbcm$ (57) space group. As a consistency check we note that $Pbcm$ is a type IIA maximal non-isomorphic subgroup of the original $Cmcm$ space group.

To determine the magnetic structure of the Er sublattice in $ErFe_6Sn_6$ we carried out a group theory analysis of the possible magnetic space groups and magnetic ordering modes derived from the $Pbcm$ space group. There are eight magnetic space groups associated with the $Pbcm$ crystal space group, as shown in table 2.

The behaviour of the magnetic moments within these magnetic space groups can be deduced by considering the character table of the mmm group which underpins these magnetic space groups (table 2). The point group of the Er 4d sites in the doubled cell is m_z and the admissible magnetic point groups of the Er 4d site are therefore the following.

- $\cdot\cdot m$ with the Er magnetic moment perpendicular to the mirror plane i.e. along the c-axis.
- $\cdot\cdot m'$ with the Er magnetic moment in the mirror plane i.e. in the ab-plane.

Now, if we denote the magnetic moment components of atom 1 (i.e. x, y, z) by μ_x, μ_y and μ_z, we deduce the moments of the remaining three 4d atoms as shown in table 3, ignoring any time-reversal operations at this stage. The final magnetic structures can then be derived from

Table 2. Character table of the *mmm* group [26].

Representation	E	C_{2x}	C_{2y}	C_{2z}	I	m_x	m_y	m_z	Magnetic space group
Γ_1^+	+1	+1	+1	+1	+1	+1	+1	+1	$Pbcm$
Γ_2^+	+1	−1	+1	−1	+1	−1	+1	−1	$Pb'cm'$
Γ_3^+	+1	+1	−1	−1	+1	+1	−1	−1	$Pbc'm'$
Γ_4^+	+1	−1	−1	+1	+1	−1	−1	+1	$Pb'c'm$
Γ_1^-	+1	+1	+1	+1	−1	−1	−1	−1	$Pb'c'm'$
Γ_2^-	+1	−1	+1	−1	−1	+1	−1	+1	$Pbc'm$
Γ_3^-	+1	+1	−1	−1	−1	−1	+1	+1	$Pb'cm$
Γ_4^-	+1	−1	−1	+1	−1	+1	+1	−1	$Pbcm'$

Table 3. Atomic positions and generating operations of the Er 4d sites (*Pbcm* setting) in $ErFe_6Sn_6$.

Atom number	X	Y	Z	Generating operation
1	x	y	1/4	Identity
				(μ_x, μ_y, μ_z)
2	$-x$	$-y$	3/4	2 (001/2) 0, 0, z
				$(-\mu_x, -\mu_y, \mu_z)$
3	$-x$	$y+\frac{1}{2}$	1/4	2 ($0\frac{1}{2}0$) 0, y, $\frac{1}{4}$
				$(-\mu_x, \mu_y, -\mu_z)$
4	x	$-y+\frac{1}{2}$	3/4	2 x, $\frac{1}{4}$, 0
				$(\mu_x, -\mu_y, -\mu_z)$

the character table for each possible magnetic space group by incorporating the characters of the generating operations, which takes into account the effects of time reversal.

We note here that

- Γ_1^+, Γ_4^+, Γ_2^- and Γ_3^- yield an m_z magnetic point group for the Er 4d sites so the magnetic moment must be parallel to the c-axis in these representations and
- Γ_2^+, Γ_3^+, Γ_1^- and Γ_4^- yield a m_z' magnetic point group for the Er 4d sites so the magnetic moment must be perpendicular to the c-axis in these representations.

As mentioned earlier, the neutron diffraction pattern at 1.5 K and the magnetization data indicate that the Er magnetic order must have both a ferromagnetic and an antiferromagnetic component. Thus, we may rule out the Γ_1^+, Γ_4^+, Γ_2^- and Γ_3^- representations since they do not support such a two-component magnetic structure. We may also rule out the Γ_1^- and Γ_4^- representations since they do not support a ferromagnetic component. Thus, we are left with either Γ_2^+ with antiferromagnetic order along the a-axis and ferromagnetic order along the b-axis or Γ_3^+ with ferromagnetic order along the a-axis and antiferromagnetic order along the b-axis.

We find the best fit to the 1.5 K neutron diffraction pattern of $ErFe_6Sn_6$ to be with the Er ferromagnetic order along [100] and the Er antiferromagnetic order along [010], corresponding to a propagation vector of $[0\frac{1}{2}0]$ in the original $Cmcm$ group. (On a practical note we mention here that GSAS does not cater for propagation vectors so we cannot directly fit $Cmcm+[0\frac{1}{2}0]$.)

The fitted Er ferromagnetic component moment is $2.6 \pm 1.0\ \mu_B$ and the antiferromagnetic component is $4.9 \pm 1.5\ \mu_B$, yielding a net Er moment at 1.5 K of $5.5 \pm 1.8\ \mu_B$. The ferromagnetic component determined by neutron diffraction is significantly less than the 5.9(1) μ_B/Er derived from magnetization (figure 3). It is clear from the diffraction patterns shown in figures 4 and 5 that the magnetic scattering in $ErFe_6Sn_6$ is weak, and while the antiferromagnetic ordering yields an isolated diffraction peak, the ferromagnetic scattering sits on strong nuclear peaks.

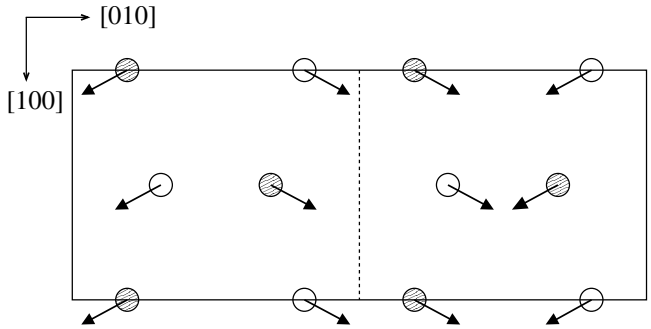

Figure 8. Magnetic structure of the Er-1 4c sublattice in $ErFe_6Sn_6$. Open circles are in the $z = \frac{1}{4}$ plane and hatched circles are in the $z = \frac{3}{4}$ plane.

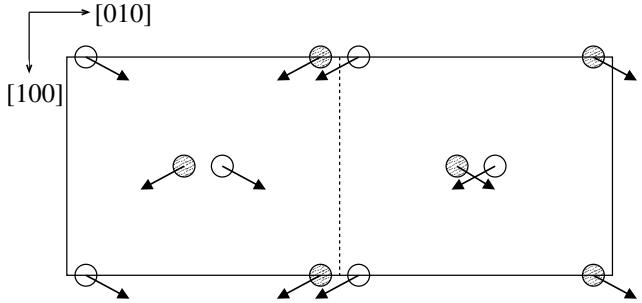

Figure 9. Magnetic structure of the Er-2 4c sublattice in $ErFe_6Sn_6$. Open circles are in the $z = \frac{1}{4}$ plane and hatched circles are in the $z = \frac{3}{4}$ plane.

In most cases the ferromagnetic contribution to a given peak is not much more than the statistical error in the observed intensity. We note, for example, that the misfits in the difference plot for the 1.5 K neutron diffraction pattern shown in figure 5 are of the same order as the clear, antiferromagnetic peak occurring at $2\theta = 11.95°$. Thus, the ferromagnetic component of the Er^{3+} moment is likely to be underestimated and a realistic uncertainty in the fitted value of 2.6 μ_B is probably at least double the 1.0 μ_B due to statistical analysis of the fitting procedure. The antiferromagnetic component of the Er^{3+} moment is more reliably determined as we are able to identify purely magnetic, albeit weak, peaks in the diffraction pattern at 1.5 K, arising from the antiferromagnetism. As we shall see in section 3.4.3, our ^{166}Er Mössbauer spectroscopy work provides a reliable measure of the *total* Er^{3+} moment, and this total moment is fully consistent with the resultant of the antiferromagnetic component taken from neutron diffraction and the ferromagnetic component from magnetization.

In figures 8 and 9 we show the magnetic ordering modes of the Er-1 and Er-2 4c sites, respectively. The magnetic space group is $Pbc'm'$ from the Γ_3^+ representation. Within the framework of the underlying $Cmcm$ family of magnetic groups, the ferromagnetic group is $Cmc'm'$ and the antiferromagnetic group is $C_Pm'cm'$.

We also obtained a diffraction pattern at 1.5 K on the E6 diffractometer, using a longer neutron wavelength of 2.447 Å to look for magnetic peaks with larger d-spacings than the $(1\frac{5}{2}0)$ peak. No discernible magnetic scattering contributions at d-spacings corresponding to the (020), $(0\frac{5}{2}0)$, (030), $(0\frac{7}{2}0)$ or (100) peaks were observed, consistent with our determined magnetic structure.

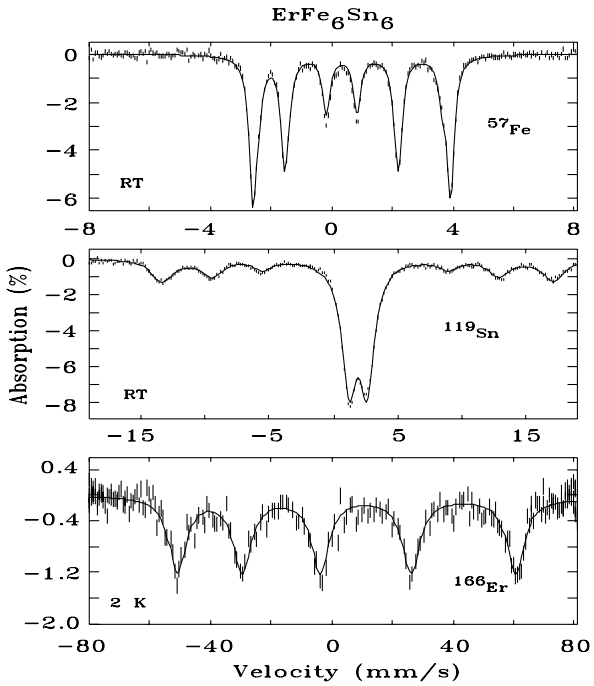

Figure 10. ^{57}Fe (top), ^{119}Sn (middle) and ^{166}Er (bottom) Mössbauer spectra of $ErFe_6Sn_6$ obtained at 295 K (^{57}Fe and ^{119}Sn) and 2 K (^{166}Er). Note the different velocity scales of these three spectra.

3.4. Mössbauer spectroscopy

3.4.1. ^{57}*Fe Mössbauer spectroscopy.* In figure 10 (top) we show the ^{57}Fe Mössbauer spectrum of $ErFe_6Sn_6$ obtained at 295 K. The ^{57}Fe Mössbauer spectra of the RFe_6Sn_6 compounds have already been published by Rao and Coey [4] and our results are in excellent agreement with theirs. Our measured ^{57}Fe average hyperfine field B_{hf} is 20.1(1) T at 295 K. We fitted the ^{57}Fe Mössbauer spectrum with two magnetically split sextets even though the $ErFe_6Sn_6$ structure contains five crystallographically inequivalent Fe sites. From a Mössbauer point of view we may treat the Fe sites as effectively magnetically equivalent, given the similarity of their magnetic environments. There is evidence to suggest that there is a direct correlation between the Wigner–Seitz (WS) cell volume and B_{hf} at the Fe sites [27] and we have calculated the WS volumes at the five Fe sites in $ErFe_6Sn_6$ using the BLOKJE program [28]. We find that the five Fe WS cell volumes all lie in the narrow range 11.4–12.1 Å^3, which supports the effective magnetic equivalence mentioned. These experimental and theoretical findings are also in agreement with band calculations carried out on YFe_6Sn_6 by Rao *et al* [29].

Our ^{57}Fe B_{hf} value of 22.9(3) T at 12 K translates into an Fe atomic magnetic moment of $2.0 \pm 5\ \mu_B$ at 12 K, using the field-to-moment conversion factor of 11.2 ± 2.5 T/μ_B, given by Häggström *et al* [30], which was derived from a compilation of Mössbauer data on a number of Fe–Ge binary compounds. Electronic structure calculations on the RFe_6Sn_6 compounds by Rao *et al* [29] yielded a conversion factor of 11.8 T/μ_B for the core electron contribution to the ^{57}Fe hyperfine field. Despite the large uncertainty in the field-to-moment conversion factor, our scaled value of $2.0 \pm 5\ \mu_B$ is fully consistent with the Fe moment of $2.4 \pm 6\ \mu_B$ derived from our neutron diffraction data at 5.3 K.

Table 4. WS cells (nearest-neighbour configurations) of the Sn sites in $ErFe_6Sn_6$.

Sn atom number	WS-cell volume (Å^3)	Er	Fe	Sn
1	20.0	2	8	5
2	20.4	1	8	7
3	19.0	3	6	3
4	21.4	0	6	9
5	19.2	3	6	3
6	21.9	0	6	9
7	21.0	0	6	9
8	19.8	3	6	3
9	21.4	1	7	7
10	21.5	1	6	7

3.4.2. ^{119}*Sn Mössbauer spectroscopy.* Sn is non-magnetic and so any hyperfine magnetic field observed at the ^{119}Sn nucleus is due to surrounding magnetic moments i.e. a transferred hyperfine field. We have determined the nearest-neighbour environments of the ten Sn sites in $ErFe_6Sn_6$ by calculating their WS cells using BLOKJE [28].

Above ∼5 K only the Fe sublattice is magnetically ordered and the WS calculations shown in table 4 indicate that the Sn sites in $ErFe_6Sn_6$ have either six, seven or eight Fe nearest neighbours. The magnetic structure of the Fe sublattice in $ErFe_6Sn_6$, determined from our neutron diffraction data, indicates that the Sn 4c sites (Sn_1 to Sn_8) have half of their neighbouring Fe moments along [100] and half antiparallel along [$\bar{1}$00], resulting in a zero transferred hyperfine field. The two Sn 8g sites (Sn_9 and Sn_{10}) have all their neighbouring Fe moments parallel which should result in a substantial transferred hyperfine field at the Sn site. The two Sn 8g sites account for exactly one-third of the Sn atoms.

In figure 10 (middle) we show the ^{119}Sn Mössbauer spectrum of $ErFe_6Sn_6$ obtained at 295 K. The spectrum comprises both a magnetically split and a non-magnetic component and the fit to the spectrum shows that 36(2)% of the Sn sites have a transferred hyperfine field of 22.2(1) T whereas the remaining 64(2)% of the Sn sites experience no net transferred hyperfine field, in excellent agreement with our deduced magnetic structure of the Fe sublattice in $ErFe_6Sn_6$.

3.4.3. ^{166}*Er Mössbauer spectroscopy.* In figure 10 (bottom) we show the ^{166}Er Mössbauer spectrum of $ErFe_6Sn_6$ obtained at 2 K. The excited nuclear state spin $= 2$ and the ground state spin $= 0$ and the spectrum is a well resolved magnetically split quintet despite the fact that there are two inequivalent Er sites in the $ErFe_6Sn_6$ structure. This supports our use of a single Er magnetic moment in the fitting of the neutron diffraction data. The experimental half-linewidth is 3.5(1) mm s^{-1}, broader than the source linewidth of 2.49(4) mm s^{-1} on the $ErFe_2$ calibration. This broadening most likely reflects the fact that the $ErFe_6Sn_6$ structure actually contains two crystallographically inequivalent Er sites which are unresolved by ^{166}Er Mössbauer spectroscopy. Er^{3+} electronic relaxation effects persisting below the Er magnetic ordering temperature may also play a role.

The isomer shift is 0.5(1) mm s^{-1}, the small value being expected for a $2 \rightarrow 0$ rotational nuclear transition.

The electric quadrupole parameter $eQV_{ZZ} = 17.6(7)$ mm s^{-1} at the ^{166}Er nucleus. This value is larger than the 'free-ion' value of 16.3(7) mm s^{-1} [32], indicating a significant contribution to the electric field gradient from the surrounding lattice charges. The principal electric quadrupole energy term comprises two contributions, a dominant 4f term and a smaller

lattice contribution and to a first approximation in the presence of a large magnetic hyperfine field can be written, using standard notation, as

$$eQV_{ZZ} = eQV_{ZZ}^{4f} + \tfrac{1}{2}eQV_{ZZ}^{lattice}[3\cos^2\theta - 1 + \eta\sin^2\theta\cos 2\phi] \quad (1)$$

where θ and ϕ are the polar angles of the ^{166}Er hyperfine magnetic field in the principal axis system of the electric field gradient. The complete lack of data on the crystal field interactions in the RFe_6Sn_6 series precludes a more detailed analysis of the electric field gradient at the ^{166}Er nucleus in $ErFe_6Sn_6$. However, we can make the following observations: the orthorhombic point symmetry of the Er^{3+} 4c sites ($m2m$) yields a non-zero asymmetry parameter η; furthermore, the X, Y, Z principal axis system of the electric field gradient tensor must be coincident with the crystal a, b, c axes. However, we cannot determine the precise axial correspondence between the principal axes of the electric field gradient and the crystal axes.

The hyperfine magnetic field at the ^{166}Er nucleus in $ErFe_6Sn_6$ at 1.4 K is 742(5) T. The hyperfine magnetic field at a rare-earth site in an R–Fe intermetallic compound can be written as (see e.g. [31])

$$B_{hf} = B_{4f} + B_{cp} + B_p + B_{nn}^{R} + B_{nn}^{Fe} + B_{ext} \quad (2)$$

where the individual terms are the following.

- B_{4f} is the field due to the incomplete 4f electron shell. The dominant contribution is from the 4f orbital angular momentum L with a weaker dipolar contribution from the 4f spin angular momentum S. These momenta may be projected onto the total momentum to express the field in terms of $\langle J_Z\rangle$.
- B_{cp} is the core polarization field which arises from the deformations of the inner shells by the 4f shell. This field is written as

$$B_{cp} = -B_{cp}^{o}(g_J - 1)\langle J_Z\rangle \quad (3)$$

  where $B_{cp}^{o} \sim$ 6–10 T [32, 33] and g_J is the Landé g-factor of the R^{3+} ion ($g_J = 1.2$ for Er^{3+}).
- B_p is the contribution from conduction electron polarization by the spin of the parent R^{3+} ion.

$$B_p = K_p\langle S_Z\rangle = K_p(g_J - 1)\langle J_Z\rangle \quad (4)$$

  where K_p is a constant.
- B_{nn}^{R} and B_{nn}^{Fe} are transferred hyperfine fields from the surrounding R and Fe sublattices, respectively, mediated by conduction electron polarization.
- B_{ext} represents any externally applied magnetic fields.

Li *et al* [34] deduced a value of 770.0 ± 7.4 T for the total intra-ionic hyperfine field (i.e. $B_{4f} + B_{cp}$) in $ErFe_2$. The Curie temperature of $ErFe_2$ is 587 K [35] and the cubic symmetry precludes second-order crystal-field terms so the magnetic moment of the Er^{3+} ion in $ErFe_2$ as $T \to 0$ is effectively the full 9 μ_B ($=g_J J$). In fact, Li *et al* [34] calculated a $\langle J_Z\rangle$ value of 7.4956 for Er^{3+} in $ErFe_2$, including a second-order crystal-field term arising from magnetostriction effects. The full, unquenched $\langle J_Z\rangle$ value is 7.5 for Er^{3+}.

The parent conduction electron polarization field B_p can be estimated from the work of Li *et al* [34] who deduce a value of 9.4 ± 1.4 T for K_p in $ErFe_2$.

We may estimate the transferred hyperfine field from the Er sublattice to an Er site by noting that our magnetization measurement yields a ferromagnetic Er moment component of 5.9 μ_B/Er^{3+} ion. The corresponding field in $ErFe_2$ is 5.1 ± 1.3 T [34] for an Er^{3+} moment of

9 μ_B, and if we assume that this transferred field scales with the Er sublattice magnetization we obtain a value of 0.7 T for B_{nn}^{Er} in $ErFe_6Sn_6$, using a lattice parameter of 7.283 Å for $ErFe_2$ [35].

We can assume that the transferred hyperfine field from the Fe sublattice to an Er site is zero since the Fe sublattice is antiferromagnetic and we have amply demonstrated that the Er and Fe sublattices are magnetically independent. Finally, we have no externally applied magnetic fields.

Thus, our experimentally determined ^{166}Er hyperfine magnetic field value of 742(5) T translates to $\langle J_Z \rangle = 7.1$ which corresponds to an Er^{3+} magnetic moment of 8.5(1) μ_B. This value is significantly larger than the 5.5 ± 1.8 μ_B determined by neutron diffraction alone. However, as discussed in section 3.3.2, the *ferromagnetic* component of the Er^{3+} moment is more reliably determined from our magnetization measurements (5.9 ± 0.1 μ_B). Combining this value with the antiferromagnetic component provided directly by neutron diffraction (4.9 ± 1.5 μ_B) yields a total Er^{3+} moment of 7.7 ± 1.5 μ_B, which is fully consistent with our direct determination of 8.5(1) μ_B for the total Er^{3+} moment by ^{166}Er Mössbauer spectroscopy.

4. Conclusions

The Fe sublattice in $ErFe_6Sn_6$ is antiferromagnetic with a Néel temperature of 560(5) K. We have used high-resolution neutron powder diffraction to show that the direction of Fe magnetic order is [100] and the Fe magnetic moment (at 5.3 K) is 2.4(6) μ_B. The Er sublattice orders magnetically at 4.8(4) K and comprises a ferromagnetic component along [100] and an antiferromagnetic component along [010]. The magnetic cell is doubled along the *b*-axis, relative to the crystal cell. The two ordered components at 2 K are 5.9 ± 0.1 μ_B (ferromagnetic component derived from magnetization measurements) and 4.9 ± 1.5 μ_B (antiferromagnetic component derived from neutron diffraction). The total Er^{3+} magnetic moment deduced by ^{166}Er Mössbauer spectroscopy is 8.5(1) μ_B/Er^{3+} The magnetic ordering processes of the Er and Fe sublattices are independent of each other.

Acknowledgments

JMC wishes to acknowledge the hospitality of the Centre for the Physics of Materials, Department of Physics, McGill University, Montreal, Canada, where some of this work was carried out during a sabbatical visit. JMC is also grateful to A S Wills for useful discussions on representation analysis and for provision of the SARA*h* program. We are grateful to the staff at BENSC–Hahn–Meitner Institute for assistance during the neutron diffraction experiments. We are also grateful to Greg Kennedy and the staff of the SLOWPOKE Reactor Laboratory at Ecole Polytechnique Montréal, for neutron irradiation of the holmium targets.

This work was supported by grants from the Australian Nuclear Science and Technology Organisation, the Australian Academy of Science, the Australian Research Council; the Natural Sciences and Engineering Research Council of Canada, fonds pour la formation de chercheurs et l'aide à la recherche, Québec; Istituto Nazionale per la Fisica della Materia, Italy and the Italian MURST National Research Programme 'Alloys and intermetallic compounds: thermodynamics, physics properties and reactivity'.

References

[1] Venturini G, Welter R and Malaman B 1992 *J. Alloys Compounds* **185** 99–107
[2] Wang Y B, Wiarda D, Ryan D H and Cadogan J M 1994 *IEEE Trans. Magn.* **30** 4951–3
[3] Ryan D H and Cadogan J M 1996 *J. Appl. Phys.* **79** 6004–6

[4] Rao X L and Coey J M D 1997 *J. Appl. Phys.* **81** 5181–3
[5] Oleksyn O, Schobinger-Papamantellos P, Rodríguez-Carvajal J, Brück E and Buschow K H J 1997 *J. Alloys Compounds* **257** 36–45
[6] Schobinger-Papamantellos P, Buschow K H J, de Boer F R, Ritter C, Isnard O and Fauth F 1998 *J. Alloys Compounds* **267** 59–65
[7] Cadogan J M, Ryan D H, Swainson I P and Moze O 1998 *J. Phys.: Condens. Matter* **10** 5383–8
[8] Cadogan J M, Suharyana, Ryan D H, Moze O and Kockelmann W 2000 *J. Appl. Phys.* **87** 6046–8
[9] Häggström L, Ericsson T, Wäppling R and Chandra K 1975 *Phys. Scr.* **11** 47–54
[10] Beckman O, Carrander K, Lundgren L and Richardson M 1972 *Phys. Scr.* **6** 151–7
[11] Cadogan J M and Ryan D H 2001 *J. Alloys Compounds* **326** 166–73
[12] Hodges J A, Jehanno G, Schuhl A and Berthier Y 1981 *Hyperfine Interact.* **11** 29–35
[13] Berthier Y and Devine R A B 1981 *J. Appl. Phys.* **52** 2071–3
[14] Többens D M and Stüßer N 2001 *Neutron News* **12** 28–32
[15] Larson A C and von Dreele R B General structure analysis system *Los Alamos National Laboratory Report* LAUR 86-748
[16] Wills A S 2000 *Physica* B **276–278** 680–1 (program available from ftp://ftp.ill.fr/pub/dif/sarah/)
[17] Chafik El Idrissi B, Venturini G and Malaman B 1991 *Mater. Res. Bull.* **26** 1331–8
[18] Rao X L 1997 *PhD Thesis* University of Dublin
[19] Prandl W 1978 *Neutron Diffraction* ed H Dachs (Berlin: Springer) ch 4 pp 113–49
[20] Cadogan J M, Suharyana, Ryan D H, Moze O and Kockelmann W 2001 *IEEE Trans. Magn.* **37** 2606–8
[21] Bertaut E F and Mareschal J 1967 *Solid State Commun.* **5** 93–7
[22] Bertaut E F 1968 *Acta Crystallogr.* A **24** 217–31
[23] García-Matres E, Martínez J L and Rodríguez-Carvajal J 2001 *Eur. Phys. J.* B **24** 59–70
[24] Olés A, Kajzar F, Kucab M and Sikora W 1976 *Magnetic Structures Determined by Neutron Diffraction* (Warszawa: Polska Akademia Nauk)
[25] Hahn T (ed) 1996 *International Tables for Crystallography* vol A, 4th edn (Dordrecht: Kluwer)
[26] Joshua S J 1991 *Symmetry Principles and Magnetic Symmetry in Solid State Physics* (Bristol: Hilger)
[27] Grandjean F, Long G J, Pringle O A and Fu J 1990 *Hyperfine Interact.* **62** 131–46
[28] Gelato L 1982 *J. Appl. Crystallogr.* **14** 151–3
[29] Rao X L, Cullen J, Skumryev V and Coey J M D 1998 *J. Appl. Phys.* **83** 6983–5
[30] Häggström L, Ericsson T, Wäppling R and Karlsson E 1975 *Phys. Scr.* **11** 55–9
[31] McCausland M A H and Mackenzie I S 1979 *Adv. Phys.* **28** 305–456
[32] Bleaney B 1979 *Magnetic Properties of Rare Earth Metals* ed R J Elliott (London: Plenum) ch 8
[33] Netz G 1986 *Z. Phys.* B **63** 343–9
[34] Li Y, Carboni C, Ross J W, McCausland M A H and Bunbury D St P 1996 *J. Phys.: Condens. Matter* **8** 865–75
[35] Buschow K H J 1977 *Rep. Prog. Phys.* **40** 1179–256